Available online at www.sciencedirect.com
SCIENCE DIRECT®
Estuarine, Coastal and Shelf Science 62 (2005) 75–94
ESTUARINE COASTAL AND SHELF SCIENCE
www.elsevier.com/locate/ECSS

SeaWiFS retrievals of chlorophyll in Chesapeake Bay and the mid-Atlantic bight

Lawrence W. Harding Jr.[a,b,*], Andrea Magnuson[a], Michael E. Mallonee[a]

[a]Horn Point Laboratory, University of Maryland, Center for Environmental Science, Box 775, Cambridge, MD 21613, USA
[b]Maryland Sea Grant College, University of Maryland, 4321 Hartwick Road, Suite 300, College Park, MD 20740, USA

Received 26 June 2004; accepted 13 August 2004

Abstract

This paper presents three years (1998–2000) of chlorophyll *a* (chl *a*) data from the *Sea*-viewing *Wi*de *F*ield-of-view *S*ensor (SeaWiFS) for Case 2 waters of Chesapeake Bay and the middle Atlantic bight (MAB) to describe phytoplankton dynamics on seasonal to interannual time scales. We used extensive data on inherent and apparent optical properties in conjunction with satellite retrievals to: (1) characterize the bio-optical properties of the study area relevant to processing and interpreting SeaWiFS data; (2) test the applicability of the SeaWiFS bio-optical algorithm (OC4v.4) for the estuarine and coastal waters; (3) evaluate the accuracy of the SeaWiFS remote sensing reflectance (R_{RS}) and chl *a* products on regional and seasonal bases using in situ observations. The characteristically strong absorption by chromophoric dissolved organic matter (a_{cdom}) and non-pigmented particulate matter (a_d) in estuarine and coastal waters contributed to overestimates of chl *a* using OC4v.4 applied to in situ radiances for the Bay (mean ratio 1.42 ± 1.20) and the MAB (2.60 ± 1.36). Values of R_{RS} from SeaWiFS in the blue region of the spectrum were low compared to in situ R_{RS}, suggesting that uncertainties remain in atmospheric correction. Direct comparisons of SeaWiFS retrievals of chl *a* with in situ chl *a* for the Bay showed larger biases and uncertainties (mean ratio 1.97 ± 1.85) than for chl *a* estimated from OC4v.4 applied to in situ R_{RS}. The larger biases were attributed to errors in SeaWiFS radiances and the larger uncertainties to time-space "aliasing" of satellite observations and in situ measurements. To reduce the time differences between SeaWiFS and in situ data, we compared chl *a* obtained from continuous underway fluorometric measurements on selected ship tracks to SeaWiFS chl *a* and showed that SeaWiFS captured phytoplankton dynamics in much of the Bay. The agreement of SeaWiFS chl *a* with in situ chl *a* was strongest in the mid- (regions 3, 4) to lower Bay (regions 1, 2), and deteriorated toward the upper Bay (regions 5, 6), in part due to a reduction of sensitivity and an increase of noise for SeaWiFS products in the highly absorbing, low R_{RS} waters of the upper Bay. A three-year time-series of SeaWiFS and in situ data showed that SeaWiFS accurately and reliably captured seasonal and interannual variability of chl *a* associated with variations of freshwater flow. Significant short-term variability of chl *a* in summer that was unresolved with shipboard data was detected in the SeaWiFS time-series and the implications are discussed. The overall performance of SeaWiFS in the mid- to lower Bay and the MAB, combined with high spatial (~ 1 km^2) and temporal (~ 100 clear scenes per year) resolution, indicate current SeaWiFS products are valuable for quantifying seasonal to interannual variability of chl *a* in estuarine and coastal waters.
© 2004 Elsevier Ltd. All rights reserved.

Keywords: remote sensing; SeaWiFS; bio-optics; case 2 algorithms

1. Introduction

Estuarine and coastal ecosystems typically express high spatial and temporal variability of phytoplankton biomass as chlorophyll (chl *a*) and primary productivity

* Corresponding author.
E-mail address: larry@hpl.umces.edu (L.W. Harding Jr.).

0272-7714/$ - see front matter © 2004 Elsevier Ltd. All rights reserved.
doi:10.1016/j.ecss.2004.08.011

(PP) (cf. Cloern, 2001). We have long recognized the role of physical forcing by factors including freshwater flow in regulating phytoplankton dynamics of these rich ecosystems (cf. Malone, 1992; Harding et al., 2002). Recent attention has focused on regional climate and weather patterns that produce variability of nutrients, dissolved organic matter (DOM), and suspended particulate matter (SPM) traceable to freshwater flow (Najjar, 1999). Shipboard data have been used for decades to characterize phytoplankton dynamics, but this approach often provides only seasonal coverage with limited spatial resolution. A potential solution to this problem of under-sampling uses remote sensing of ocean color to estimate chl *a* as a measure of phytoplankton biomass. Significant contributions have been made to our understanding of coastal phytoplankton dynamics using remote sensing and shipboard measurements of bio-optical properties (Stumpf and Tyler, 1988; Stumpf and Pennock, 1989; Gould and Arnone, 1997; Woodruff et al., 1999; Del Castillo et al., 2001; Gould et al., 2001; Tang et al., 2003). Recent developments in satellite imagery, such as the extensive data provided by the *Sea*-viewing *Wi*de *F*ield-of-view *S*ensor (SeaWiFS), have resulted in global coverage at approximately 2-day intervals, offering the opportunity to develop climate data records on key ecosystem properties. It is now reasonable to expect up to 100 relatively cloud-free SeaWiFS scenes per year for a given region of the ocean, greatly exceeding the temporal resolution that can be obtained using other approaches.

Our group has a long-standing interest in phytoplankton dynamics of Chesapeake Bay (cf. Harding, 1994; Harding and Perry, 1997; Harding et al., 1986, 1999, 2002), a large and productive estuary on the east coast of the U.S. that supports valuable fisheries (Houde and Rutherford, 1993). The annual cycle of phytoplankton in Chesapeake Bay consists of a winter–spring bloom of diatoms comprising the chl *a* maximum (Malone, 1992; Harding, 1994; Harding et al., 1999), followed by a summer maximum of picoplankton and flagellates coinciding with the PP maximum (Malone et al., 1991; Harding et al., 1986, 2002). The timing, position, and magnitude of the spring bloom are strongly driven by the spring freshet from the Susquehanna River, the largest source of freshwater and dissolved inorganic nutrients to the estuary (Malone et al., 1983, 1988; Fisher et al., 1988, 1992; Harding et al., 1986, 2002), and the summer flora largely depends on regenerated nutrients derived from metabolism of the spring bloom to support high PP (cf. Malone, 1992). Superimposed on the annual cycles of chl *a* and PP is variability associated with frontal features and tides (Cloern et al., 1983, 1989; Dunstan and Pinckney, 1989; Seliger et al., 1981; Hood et al., 1999), lateral gradients driven by estuarine circulation (Malone et al., 1986; Weiss et al., 1997), and the autecology of individual bloom-forming species (Tyler et al., 1982; Coats and Harding, 1988; Harding and Coats, 1988). Shipboard observations that support our understanding of the annual cycle of phytoplankton are relatively ineffective to characterize variability on these small spatial and temporal scales, and we have augmented in situ sampling with aircraft remote sensing of ocean color to estimate chl *a* on a series of flights conducted since the late 1980s (Harding et al., 1992, 1994, 1995). These data give increased spatial and temporal resolution and have been used to analyze the relationships of chl *a* and PP to freshwater flow and nutrient loading.

The promise of increased spatial and temporal resolution of chl *a* from SeaWiFS is complicated by Case 2 bio-optical properties of Chesapeake Bay and the middle Atlantic bight (MAB) where multiple constituents significantly affect water-leaving radiance (L_W) and remote sensing reflectance (R_{RS}). The bio-optical signature is defined by a complex mix of constituents, including abundant detritus and chromophoric dissolved organic matter (CDOM) (cf. Blough et al., 1993), potentially affecting SeaWiFS retrievals of chl *a* from a radiance ratio algorithm (OC4v.4) relating R_{RS} and chl *a* (O'Reilly et al., 1998, 2000). Atmospheric correction of SeaWiFS data using bands in the near infrared (NIR) to determine the aerosol contribution to reflectance in the visible region of the spectrum is more difficult for estuarine and coastal waters (Gordon and Wang, 1994; Gordon, 1997). L_W is assumed to be zero in the NIR because of strong absorption by pure water, but this "black pixel" assumption may not be valid for waters with high phytoplankton biomass, high turbidity, or where bottom reflectance is significant (Ruddick et al., 2000; Siegel et al., 2000). Thus, part of the satellite signal that emanates from the water column may be inappropriately attributed to the atmosphere such that L_Ws from SeaWiFS are too low or negative, requiring the implementation of additional corrections (Siegel et al., 2000; Bailey et al., 2003; O'Reilly and Yoder, 2003). The presence of highly absorbing aerosols in nearshore regions also complicates atmospheric correction, but detection of absorbing aerosols is problematic as their contribution to reflectance in the visible cannot be predicted from measurements in the NIR. These several issues are relevant to the performance of SeaWiFS in estuarine and coastal waters, accentuating the need to undertake extensive validation with in situ bio-optical data prior to using data from SeaWiFS to quantify phytoplankton dynamics.

In this paper, we draw on SeaWiFS retrievals of chl *a* to describe spatial and temporal variability of phytoplankton biomass in Chesapeake Bay and the MAB on event to interannual times scales for three consecutive years. We lead the presentation of satellite data with an analysis of in situ measurements of absorption by dissolved and particulate components, and evaluate the

influence on attenuation, reflectance, and the performance of OC4v.4. Next, we present comparisons of SeaWiFS-derived R_{RS} and chl *a* with in situ data to determine the regions of the Bay and the seasons of the year for which SeaWiFS products are reliable. An extensive time-series of SeaWiFS chl *a* is combined with field observations for 3 years of distinct freshwater flow and nutrient loading, 1998–2000. We show that: (1) the mid- to lower Bay is highly sensitive to freshwater flow and nutrient loading on seasonal and interannual time scales; (2) SeaWiFS coverage minimizes biases in quantifying phytoplankton biomass that are typical of abbreviated cruise coverage by giving a higher frequency of chl *a* retrievals; (3) short-term variability during the low-biomass summer period is better captured using SeaWiFS than shipboard sampling. This work also provides a starting point to evaluate improvements of bio-optical and atmospheric correction algorithms for these and other Case 2 waters.

2. Materials and methods

2.1. Shipboard sampling

2.1.1. Cruises

Shipboard data were obtained on research and monitoring cruises from 1996 to 2000 in Chesapeake Bay and the MAB (Fig. 1, Table 1). Measurements of bio-optical properties and chl *a* in the Bay were made seasonally (April, July–August, and October) from 1996 to 2000 as part of the NSF Land Margin Ecosystem Research (LMER) Trophic Interactions in Estuarine Systems (TIES) program. Cruises in adjacent waters of the MAB were conducted in August 1996, May 1997, August 1997, and September 1998, supporting collection of the same suite of bio-optical and chl *a* measurements. Monitoring cruises of the EPA Chesapeake Bay Program (CBP) also provided monthly or bi-monthly measurements of water quality including chl *a*. Field sampling that coincided with the operational period of SeaWiFS is summarized in Fig. 2. Data on freshwater flow, total nitrogen (TN), and total phosphorus (TP) from the Susquehanna River were acquired from the U.S. Geological Survey (USGS) as part of the National Water Quality Assessment (NAWQA) program (Leahy et al., 1990).

Table 1
Geographic coordinates of regions used in analyses of SeaWiFS and in situ data

Location	Latitude (°N)	Longitude (°W)
Region 1	36.9–37.4	75.9–76.4
Region 2	37.4–37.8	75.7–76.4
Region 3	37.8–38.4	75.6–76.4
Region 4	38.4–38.8	76.0–76.5
Region 5	38.8–39.1	76.2–76.5
Region 6	39.1–39.7	76.2–76.4
Inshore MAB	36.8–39.0	74.5–76.0
Offshore MAB	35.6–38.8	72.8–75.8

2.1.2. Discrete samples

Spectral absorption coefficients for CDOM (a_{cdom}), and pigmented (a_{ph}) and non-pigmented (a_d) particulate

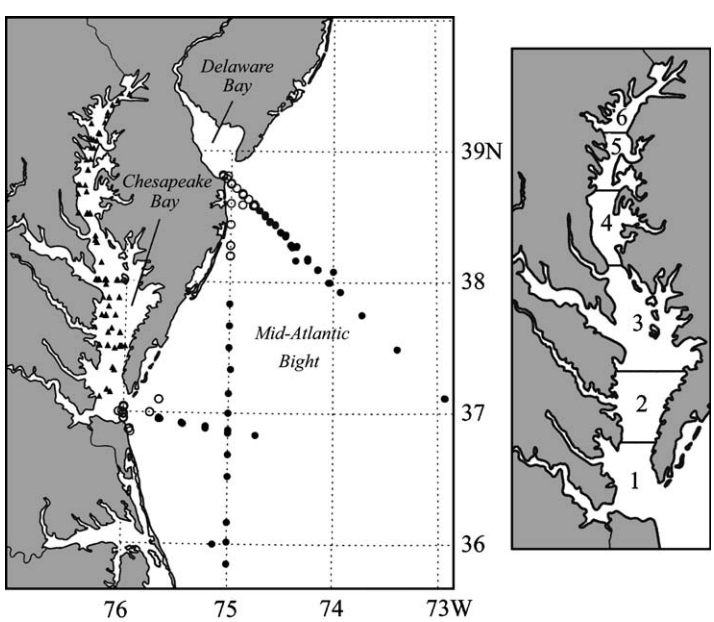

Fig. 1. Left panel: Chesapeake Bay and the adjacent MAB showing station locations for bio-optical measurements from 1996 to 2000. Right panel: Chesapeake Bay divided into six regions referred to in text. Regions 1 and 2, lower Bay; regions 3 and 4, mid-Bay; and regions 5 and 6, upper Bay. Symbols represent Chesapeake Bay (triangles), inshore MAB (open circles), offshore MAB (closed circles).

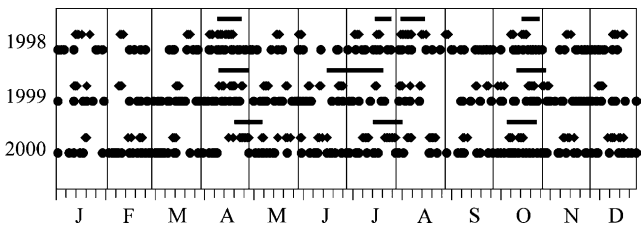

Fig. 2. Temporal coverage of in situ bio-optical measurements (dashes), in situ chl *a* measurements (diamonds), and cloud-free SeaWiFS images (circles) for each year of the time-series.

fractions were determined for surface samples collected at ~10–15 stations on each LMER-TIES cruise. Sample collection, preparation, and measurements were made according to the Ocean Optics Protocols for SeaWiFS Validation (Fargion and Mueller, 2000). Seawater samples were filtered through 0.2 μm cellulose syringe filters for the determination of a_{cdom}. The absorbance of the filtrate was measured in 10 cm cuvettes on an HP8452A Diode Array spectrophotometer (190–820 nm) against a blank of Milli-Q water. A null point correction was made by subtracting average absorbance for a wavelength interval between 720 and 780 nm that was selected by examining each spectrum individually. $a_{\mathrm{cdom}}(\lambda)$ was calculated as:

$$a_{\mathrm{cdom}}(\lambda) = \frac{2.303\mathrm{OD_s}(\lambda)}{l} \tag{1}$$

where $\mathrm{OD_s}(\lambda)$ is the optical density of the sample after the null point correction and l is the pathlength of the cuvette. Spectral absorption coefficients of particulate material were measured by the filter pad method (Mitchell, 1990). Particulate samples were concentrated on Whatman GF/F filters, and absorbance measurements were made on a Shimadzu UV-2401PC UV-VIS dual-beam spectrophotometer (300–800 nm). Hot methanol extraction (Kishino et al., 1985) was used to distinguish pigmented (e.g., phytoplankton) and non-pigmented (e.g., both organic and inorganic particles) components of absorption. Despite the inevitable presence of mineral particles, the non-pigmented fraction is referred to as "detritus" for simplicity. Spectral absorption coefficients for particulate samples were calculated from optical density spectra according to:

$$a(\lambda) = \frac{2.303A}{\beta V}\mathrm{OD_f}(\lambda) \tag{2}$$

where A is the effective area of the filter, β is the pathlength amplification factor, V is the volume of seawater filtered, and $\mathrm{OD_f}(\lambda)$ is the optical density of the filter pad after a scattering correction was applied by subtracting the average absorbance for 720–780 nm. An empirical value of β was determined for the Shimadzu spectrophotometer based on an analysis of five algal suspensions from Chesapeake Bay ranging up to 0.6 OD, following the work of Cleveland and Weidemann (1993). Estimates of a_{ph} were calculated by difference ($a_{\mathrm{ph}} = a_{\mathrm{p}} - a_{\mathrm{d}}$). Chl *a* and phaeopigment concentrations in surface waters were determined by standard fluorometric analyses (Strickland and Parsons, 1972) at ~60 stations on each LMER-TIES cruise. Additional measurements of chl *a* were acquired from the CBP database.

2.1.3. In situ radiometric measurements

Vertical profiles of spectral downwelling irradiance (E_{d}) and upwelling radiance (L_{u}) at 13 wavebands (412, 443, 455, 490, 510, 532, 550, 560, 589, 625, 671, 683, 700 nm) were obtained at ~10–15 stations on each LMER-TIES cruise using a Bio-Spherical Instruments (San Diego, California, USA) MER-2040 following appropriate protocols (Fargion and Mueller, 2000). A deck cell radiometer (MER-2041) simultaneously measured downwelling surface irradiance (E_{s}) at the same wavebands. All profile data were normalized to deck measurements to account for cloud variability. Attenuation coefficients for downwelling irradiance (K_{d}) or upwelling radiance (K_{u}) were determined by simple linear regression of the natural logarithm of E_{d} or L_{u} on depth (Smith and Baker, 1984, 1986). Surface values of E_{d} ($E_{\mathrm{d}}0^-$) and L_{u} ($L_{\mathrm{u}}0^-$) were obtained by extrapolation of the regressions to the surface. Instrument self-shading corrections were applied to all $L_{\mathrm{u}}0^-$ measurements to compensate for errors associated with shading of the sensor's field-of-view by the radiometer housing (Gordon and Ding, 1992; Fargion and Mueller, 2000). $E_{\mathrm{d}}0^-$ values were transmitted through the air–sea interface assuming a constant transmission factor as:

$$E_d0^+ = \frac{E_d0^-}{0.98} \tag{3}$$

$L_{\mathrm{u}}0^-$ values were transmitted through the air–sea interface to L_{W} (Austin, 1974) as:

$$L_{\mathrm{W}} = 0.54L_{\mathrm{u}}0^- \tag{4}$$

R_{RS} values were calculated as:

$$R_{\mathrm{RS}} = \frac{L_{\mathrm{W}}}{E_{\mathrm{S}}} \tag{5}$$

2.1.4. Continuous underway measurements

Continuous underway measurements of surface salinity and chl *a* fluorescence were obtained from the flow-through Serial ASCII Instrumentation Loop (SAIL) system aboard the R/V *Cape Henlopen*. The SAIL system was equipped with Sea-Bird sensors for salinity and a Turner Designs Model 10 fluorometer for chl *a*. Discrete samples were collected from the ship's hull pump to calibrate sensors on the SAIL system.

2.2. SeaWiFS imagery

SeaWiFS Level 1a HRPT images of the Chesapeake Bay and the MAB were obtained from the Goddard Space Flight Center Earth Sciences Data and Information Services Center Distributed Active Archive Center (GES DISC DAAC). Level 1a images were processed to Level 2 using SeaWiFS Data Analysis System (SeaDAS) software version 4.3 with the NIR atmospheric correction option modified for the fourth reprocessing (Bailey et al., 2003). All of the standard masks were used, including those for land, cloud, glint, stray light, and high light. Pixels with $\theta > 56.0°$ were masked to avoid large atmospheric paths. The resulting time-series consisted of 101, 97, and 123 relatively cloud-free images for 1998, 1999, and 2000, respectively.

2.3. Matches

We used specific criteria to develop matches of SeaWiFS imagery and in situ radiometric and chl *a* observations. The "unfiltered" in situ data set consisted of 145 bio-optical observations. Our first criterion was to identify matches of satellite overpasses with in situ sampling dates. We had 93 same-day matches. The second criterion was to impose a limit of ± 3 h of sampling time from the satellite overpass. We had 41 matches within this time window. The third criterion was that at least half the pixels in a 5×5 pixel box were valid (i.e., non-zero). A pixel could be zero due to a land mask, cloud cover, or failure of atmospheric correction. We opted to set the stray light mask "off" to avoid precluding nearshore pixels that were often valid in the Bay. The combination of these criteria left 20 stations with at least 13 valid pixels. The final criterion was that the coefficient of variation (CV) was less than 0.4. The effect of this criterion differed by waveband (i.e., blue bands had higher CV), and left the sample sizes for matches we present here.

3. Results

3.1. Bio-optical properties

a_{cdom} (440), a_d (440), and a_{ph} (440) ranged from 0.1 to 1.0 m^{-1} in Chesapeake Bay and were an order of magnitude lower in the MAB (Fig. 3a–h). a_{cdom} (440) ranged from 0.2 to 0.8 m^{-1} and decreased progressively along the salinity gradient of the Bay (Fig. 3a). The essentially conservative distribution of a_{cdom} (440) along the axis of the Bay was consistent with a predominantly terrestrial origin of CDOM (cf. Rochelle-Newall and Fisher, 2002; Magnuson et al., 2004). Mean a_{cdom} (440) for each cruise ranged from ~0.31 to 0.74 and showed variability related to the seasonality of flow. a_d dominated absorption at low salinities in the upper Bay (regions 5 and 6), and declined seaward at salinities greater than 10 (Fig. 3c). a_d (440) and a_{ph} (440) were more variable than a_{cdom} (440), with high spatial variability obscuring seasonal and interannual patterns (Fig. 3c,e). Seasonal and interannual distributions of a_{ph} (440) varied along the salinity gradient, with highest values occurring at salinities of 10–15 where the chl *a* maximum was typically observed. The magnitudes of a_{cdom} (440), a_d (440), and a_{ph} (440) were comparable in the Bay and inshore waters of the MAB (compare filled and open circles in Fig. 3a–f), with each component contributing significantly to total water column absorption (a_T). a_{cdom} dominated a_T in offshore waters of the MAB (Fig. 3b), with lower contributions of a_{ph} and a_d to a_T (Fig. 3d,f).

The distributions of a_T, K_d, and R_{RS} in the Bay and MAB coincided with distributions of dissolved and particulate materials (Figs. 4g,h and 5; Table 2). Strong absorption by CDOM, detritus, and phytoplankton contributed to K_d (490) values >1 m^{-1}, with values sometimes ≥ 6 m^{-1} in the upper Bay (Fig. 3g). R_{RS} (λ) maxima occurred in the green region of the spectrum where dissolved and particulate materials absorb weakly, whereas R_{RS} (λ) minima occurred in the blue region of the spectrum where dissolved and particulate materials absorb strongly (Fig. 4). There was a shift in the wavelength of maximum R_{RS} (λ) from 589 nm in the mid- to upper Bay, to 560 nm in the lower Bay and inshore MAB, to 490 nm in the offshore MAB (Fig. 4), as the combined absorption due to CDOM, detritus, and phytoplankton decreased with latitude in the Bay and with distance offshore (Fig. 3a–h). The magnitude of R_{RS} (λ) was highly variable in oligohaline and polyhaline regions, with lower values and less variability in the mesohaline region of the Bay.

3.2. OC4v.4 performance in Chesapeake Bay – MAB

SeaWiFS retrievals of chl *a* were obtained from OC4v.4 applied to satellite-derived radiances according to Eq. (6):

$$\text{chl } a = 10.0^{\left(0.366 - 3.067 R_{max} + 1.930 R_{max}^2 + 0.649 R_{max}^3 - 1.532 R_{max}^4\right)} \quad (6)$$

where $R_{max} = \log_{10}\left(R_{RS555}^{443} > R_{RS555}^{490} > R_{RS555}^{510}\right)$ (O'Reilly et al., 2000). We tested the applicability of this algorithm to Chesapeake Bay and the MAB using in situ measurements of R_{RS} (λ) as inputs to OC4v.4 and compared the outputs to in situ chl *a*. OC4v.4 applied to in situ R_{RS} (λ) overestimated chl *a* by ~42% in the Bay with an uncertainty of more than a factor of two, and by ~160% in the MAB, also with an uncertainty of more than a factor of two (Fig. 5a).

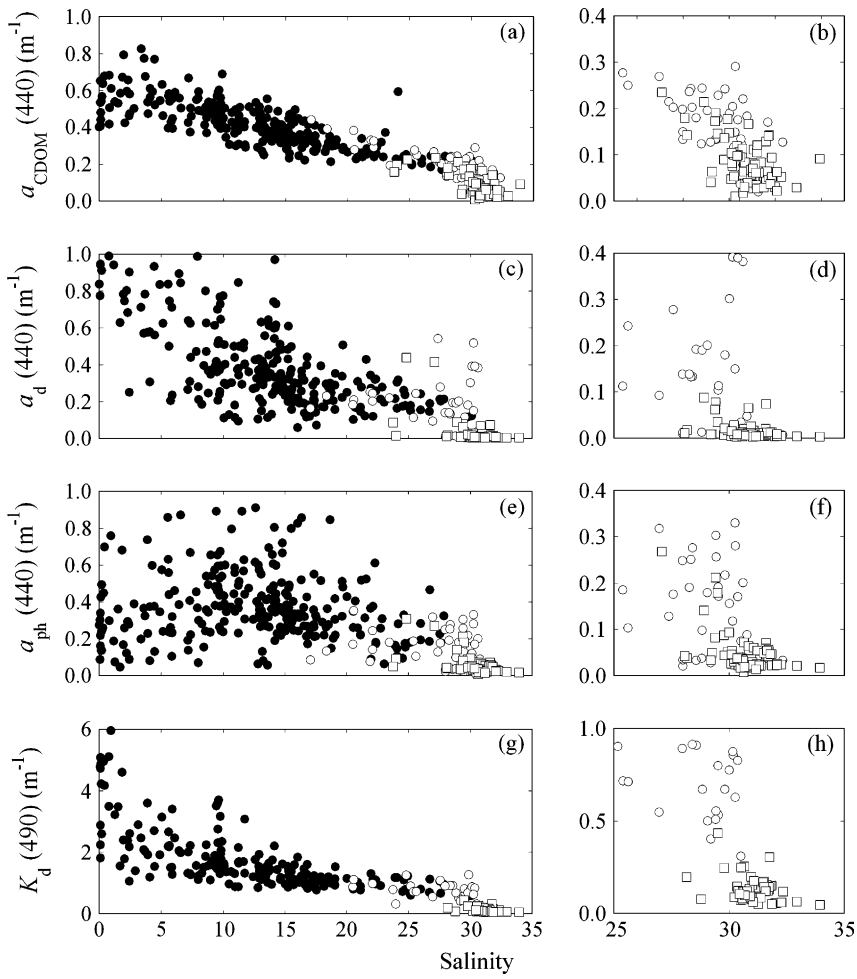

Fig. 3. (a–h) Distributions of $a_{cdom}(440)$, $a_d(440)$, $a_{ph}(440)$, and K_d490 with respect to salinity for Chesapeake Bay (filled circles), inshore MAB (open circles), and offshore MAB (squares). Right panels provide an expanded view of data for the MAB.

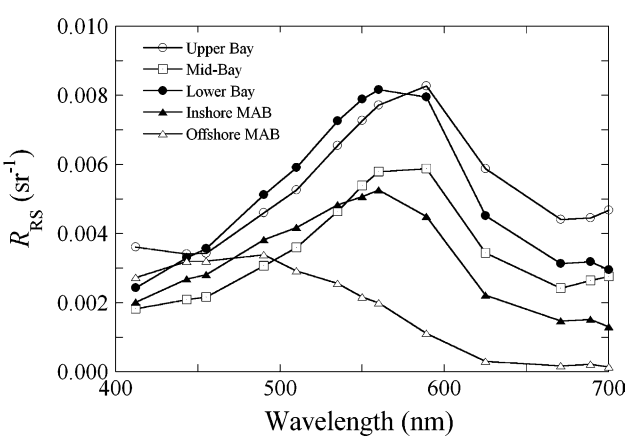

Fig. 4. Mean R_{RS} spectra for regions in Chesapeake Bay and the MAB.

3.3. SeaWiFS – in situ comparisons

We compared retrievals of chl *a* using OC4v.4 applied to in situ R_{RS} and to SeaWiFS R_{RS} with in situ chl *a* from shipboard sampling (Fig. 5a,b). OC4v.4 applied to in situ R_{RS} overestimated in situ chl *a* by about 42% (Fig. 5a), whereas SeaWiFS overestimated in situ chl *a* by ~100% (Fig. 5b) for Chesapeake Bay. This difference represents increases of ~40% for both bias and uncertainty compared to chl *a* predicted by OC4v.4 applied to in situ R_{RS}, suggesting that uncertainty of SeaWiFS retrievals may be associated with remaining errors in satellite-derived radiances. The same analysis for the MAB showed no increases of bias or uncertainty for SeaWiFS chl *a* compared to chl *a* retrieved from OC4v.4 applied to in situ R_{RS} (Fig. 5a,b).

In situ R_{RS} for each station were compared to mean values of SeaWiFS R_{RS} for 25-pixel boxes centered on the stations we occupied for shipboard profiles. Means of the ratios of SeaWiFS to in situ R_{RS} ranged from 0.81 at 412 nm to 1.06 at 670 nm (Fig. 6a–f). The larger differences between SeaWiFS and in situ R_{RS} for wavebands in the blue region of the spectrum may reflect errors in the atmospheric correction of SeaWiFS radiances, related to a violation of the black pixel assumption or the presence of absorbing aerosols. An

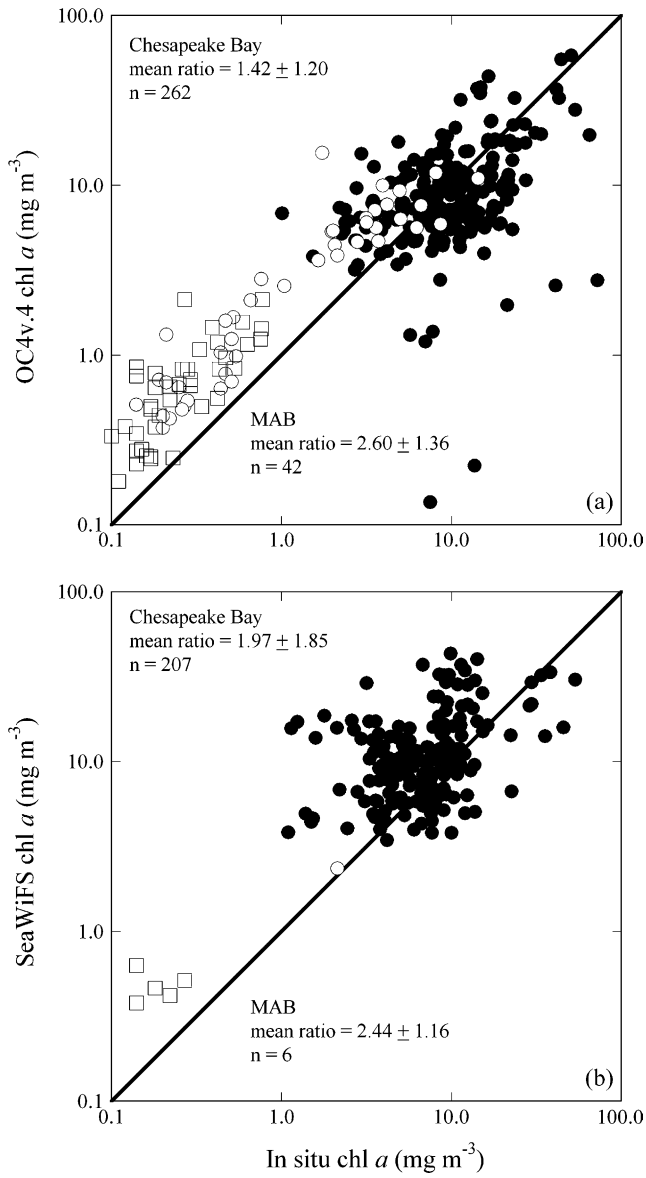

Fig. 5. (a,b) Comparisons of in situ chl *a* to: (a) chl *a* estimated from OC4v.4 applied to in situ R_{RS}; (b) SeaWiFS retrievals of chl *a* from OC4v.4. SeaWiFS values represent the mean of a 3×3 pixel box centered on the station location for in situ sampling. A chl *a* match was considered valid if the SeaWiFS observation and in situ measurement occurred on the same day, and if half the pixels (5 of 9) in a box centered on the latitude and longitude of the station returned valid estimates. The original data set of matches contained over 1400 chl *a* observations. Mean ratio = SeaWiFS chl *a*/in situ chl *a*.

advantage of using OC4v.4 for the Bay is that 510 and 555 nm wavebands were consistently selected for R_{max}, avoiding the use of radiances that were more often underestimated by SeaWiFS. SeaWiFS chl *a* compared to in situ chl *a* from CBP and TIES cruises showed significant, positive relationships with positive bias in simple, linear regressions (Fig. 7a–c). The scatter of matches underlying these regressions decreased as we applied increasingly restrictive search criteria, from same-day (Fig. 7b) to ±3 h for satellite overpass and time of in situ sampling (Fig. 7c).

SeaWiFS retrievals of chl *a* for October 1998, October 1999, and May 2000 were compared to chl *a* obtained from continuous underway fluorescence measurements on axial transects of the Bay (Figs. 8–10a–e). Agreement of SeaWiFS chl *a* and in situ chl *a* was strong in the lower Bay with SeaWiFS capturing much of the small-scale (10s of km) variability evident in chl *a* from fluorescence measurements. SeaWiFS chl *a* was increasingly inaccurate with distance up the Bay (Figs. 8–10c), corresponding to increasingly noisy R_{RS} (555) and R_{RS} 510/555 northward along the salinity gradient (Figs. 8–10d,e). We did not expect a perfect correspondence of SeaWiFS chl *a* and in situ chl *a* because of time differences between the measurements, i.e., SeaWiFS images are synoptic and underway transects required ~24 h to complete. Nonetheless, these findings suggest a loss of accuracy for SeaWiFS chl *a* that may be associated with bio-optical properties of the turbid upper Bay (regions 5, 6), consistent with strong absorption by CDOM and detritus we observed. We omitted these regions from subsequent analyses because of the poor SeaWiFS retrievals of chl *a*.

3.4. Time-series of monthly mean chl a

Monthly means of SeaWiFS chl *a* and in situ chl *a* were used to generate time-series for the mid- to lower Bay (Fig. 11a–l). A visual inspection of these data indicated SeaWiFS overestimated in situ chl *a* from ~50% in region 1 to ~100% in region 4, while capturing seasonal and interannual patterns of chl *a* in regions 1–4. In 1998, a year of higher-than-average freshwater flow, the spring bloom was large in magnitude and spatial extent, with high chl *a* extending

Table 2
Regional mean ± SD and range (in parentheses) of salinity, chl *a*, a_T (443), K_d (490), and R_{RS} (555) for the upper Bay, mid-Bay, lower Bay, inshore MAB, and offshore MAB

Region	Salinity	chl *a* (mg m^{-3})	a_T (443) (m^{-1})	K_d (490) (m^{-1})	R_{RS} (555) (sr^{-1})
Upper Bay	6.3 ± 5.1 (0.08–23.0)	15.9 ± 23.4 (1.0–164.5)	1.78 ± 0.89 (0.79–5.39)	2.00 ± 1.21 (0.75–6.60)	0.0069 ± 0.0032 (0.0011–0.018)
Mid-Bay	12.9 ± 3.2 (5.8–19.0)	14.2 ± 10.9 (4.3–72.4)	1.04 ± 0.27 (0.60–1.87)	1.01 ± 0.37 (0.54–2.51)	0.0050 ± 0.0030 (0.0012–0.024)
Lower Bay	20.8 ± 4.9 (10.1–30.1)	10.3 ± 9.4 (2.2–51.0)	0.81 ± 0.26 (0.26–1.45)	0.83 ± 0.25 (0.40–1.69)	0.0076 ± 0.0031 (0.0017–0.018)
Inshore MAB	28.9 ± 3.2 (16.0–31.6)	4.4 ± 8.8 (0.14–44.2)	0.52 ± 0.30 (0.10–1.04)	0.41 ± 0.26 (0.08–0.99)	0.0049 ± 0.0031 (0.0016–0.012)
Offshore MAB	31.2 ± 0.81 (28.8–33.9)	0.36 ± 0.43 (0.06–3.2)	0.12 ± 0.058 (0.05–0.19)	0.10 ± 0.09 (0.04–0.62)	0.0023 ± 0.0014 (0.0012–0.010)

Field data were collected 1996–2000 at 265 stations in Chesapeake Bay, and 110 stations in the MAB.

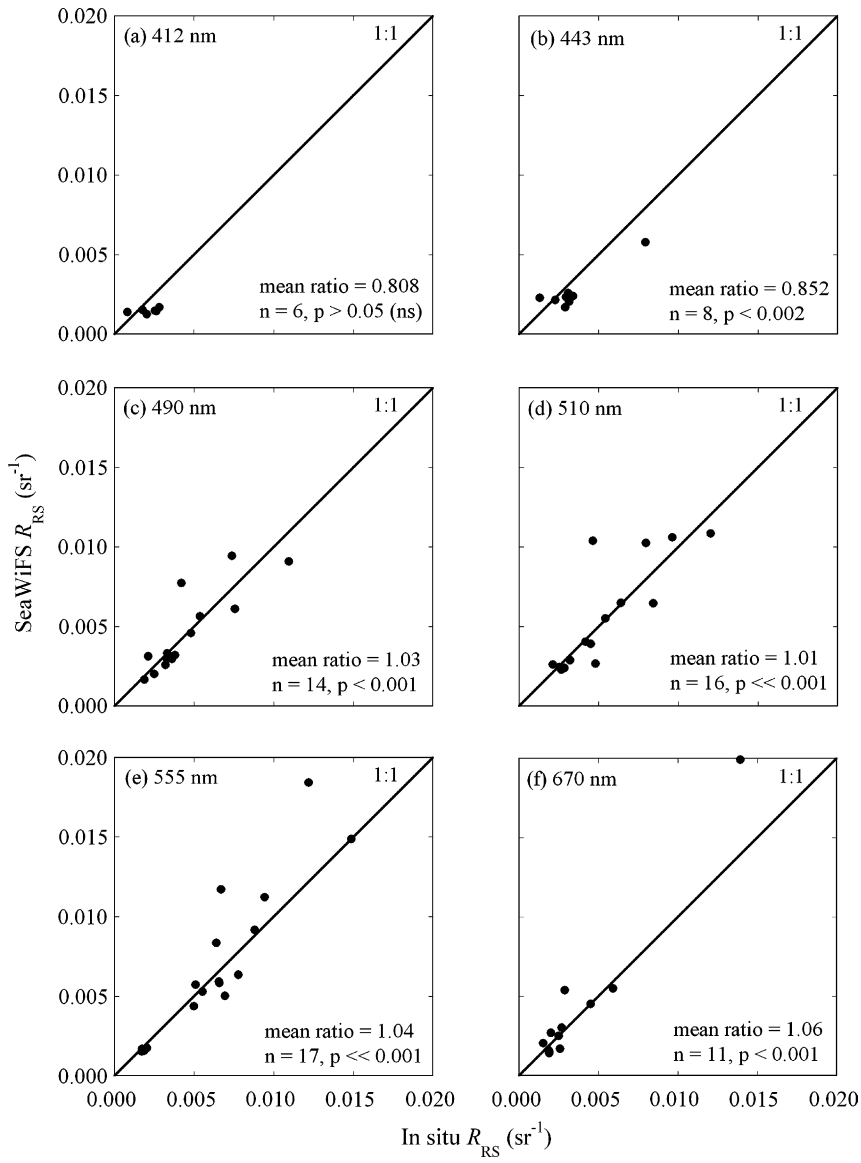

Fig. 6. (a–f) Comparisons of SeaWiFS and in situ R_{RS}. In situ R_{RS} values were compared to average SeaWiFS R_{RS} for 5×5 pixels centered on the bio-optical station. Valid matches of SeaWiFS and in situ R_{RS} were limited to a time window of ±3 h. A match was considered valid if half the pixels (13 of 25) in a box returned non-negative R_{RS} and the CV was less than 40%. The original in situ R_{RS} data set consisted of 145 observations. Mean ratio = SeaWiFS R_{RS}/in situ R_{RS}.

as far south as region 1. In 1999, a year of below-average freshwater flow, the spring bloom was smaller in magnitude and spatial extent. In 2000, a year of average freshwater flow, the bloom was relatively large in magnitude, but did not extend as far south in the Bay as it did in 1998.

We normalized the monthly means of SeaWiFS chl *a*, in situ chl *a*, and freshwater flow from the Susquehanna River to 3-year means (1998–2000) to remove bias in SeaWiFS chl *a*, and to determine the effect of freshwater flow (Fig. 12a–o). High freshwater flow in winter 1998 was followed by increased chl *a* from late winter to early spring that was most strongly expressed in the lower Bay. Contrasting periods of low freshwater flow in spring and summer 1999 led to below-average chl *a*. An unusually wet period in fall 1999 associated with several tropical storms supported an increase of chl *a* above the 3-year mean. In 2000, a year of average freshwater flow, monthly means of chl *a* fluctuated around the 3-year means, with low values in February and March following dry weather in January and February. At monthly time steps, these data suggest at most a 1-month lag in the response of chl *a* to changes in freshwater flow in spring and fall. We observed large, positive deviations of freshwater flow in summers of 1998 and 2000, but only small increases of chl *a* as the absolute magnitude of summer flow was low.

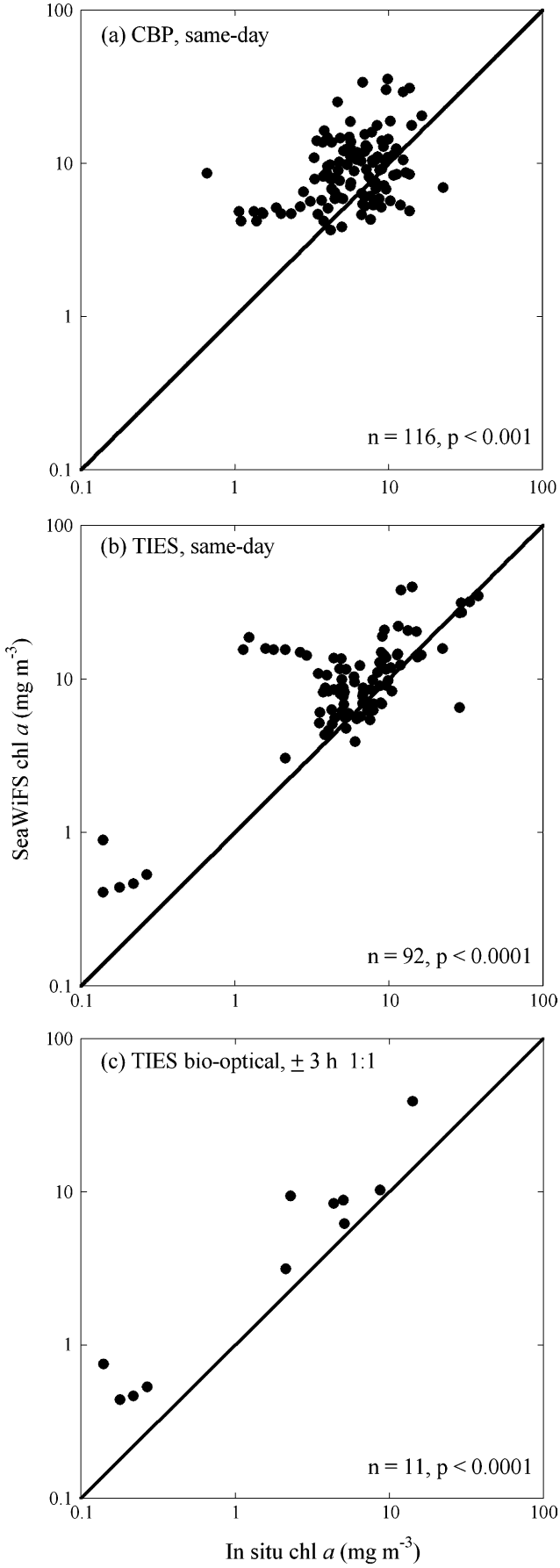

Fig. 7. (a–c) SeaWiFS chl *a* and in situ chl *a* from matches of clear-sky images and shipboard measurements at: (a) CBP cruise stations, same day as the satellite overpass; (b) LMER-TIES cruise stations, same day as the satellite overpass; (c) LMER-TIES cruise stations, ±3 h of the satellite overpass.

3.5. Frequency distributions of chl a

Frequency distributions of SeaWiFS retrievals of chl *a* and in situ chl *a* for spring (March–May) and summer (June–August) were computed from data combined for the mid- and lower Bay (regions 1–4) (Fig. 13a–g). Mean values were higher for SeaWiFS chl *a* than for in situ chl *a*, particularly in spring when in situ data contained a significant number of low chl *a* that were not retrieved by SeaWiFS. Interannual patterns of spring and summer chl *a* were similar for SeaWiFS chl *a* and in situ chl *a*, with highest mean chl *a* in 1998 and lowest mean chl *a* in 1999 from both sources (Fig. 14a–f), consistent with interannual patterns of freshwater flow (Fig. 13a–c). SeaWiFS chl *a* were log-normally distributed in summer, as were in situ chl *a*, whereas in situ chl *a* in spring were irregularly distributed, especially in 2000 (Fig. 13a–g). This may be explained by the timing and frequency of cruises in spring when chl *a* often changes 1–2 orders of magnitude in a short time period. The rapid changes of chl *a* typically observed in Chesapeake Bay are particularly evident in the frequency distributions for March, April, and May 2000 (Fig. 13g). We found the higher frequency of SeaWiFS chl *a* lessened the biases introduced by relatively sparse shipboard sampling, emphasizing an advantage of satellite remote sensing in providing data of high temporal resolution.

3.6. Time-series of daily mean chl a

Daily means of SeaWiFS retrievals of chl *a* and in situ chl *a* in region 2 were computed for 3 years to examine event-scale variability in the Bay (Fig. 14a–f). Both of these data sets captured major features of the annual cycle of phytoplankton, with SeaWiFS chl *a* providing finer temporal resolution during the development and dissipation of the spring bloom. The increased sampling frequency of SeaWiFS chl *a* allowed us to detect variability of a factor of two or more in the late spring and summer persisting for periods of days, whereas in situ chl *a* missed dynamics on this time scale. High variability of chl *a* in spring 1998 and 2000 was associated with blooms of the dinoflagellate, *Prorocentrum minimum*, in the mid-Bay that persisted for ~2 weeks, detected by SeaWiFS and aircraft ocean color measurements using a SeaWiFS Aircraft Simulator (SAS III; http://www.cbrsp.org).

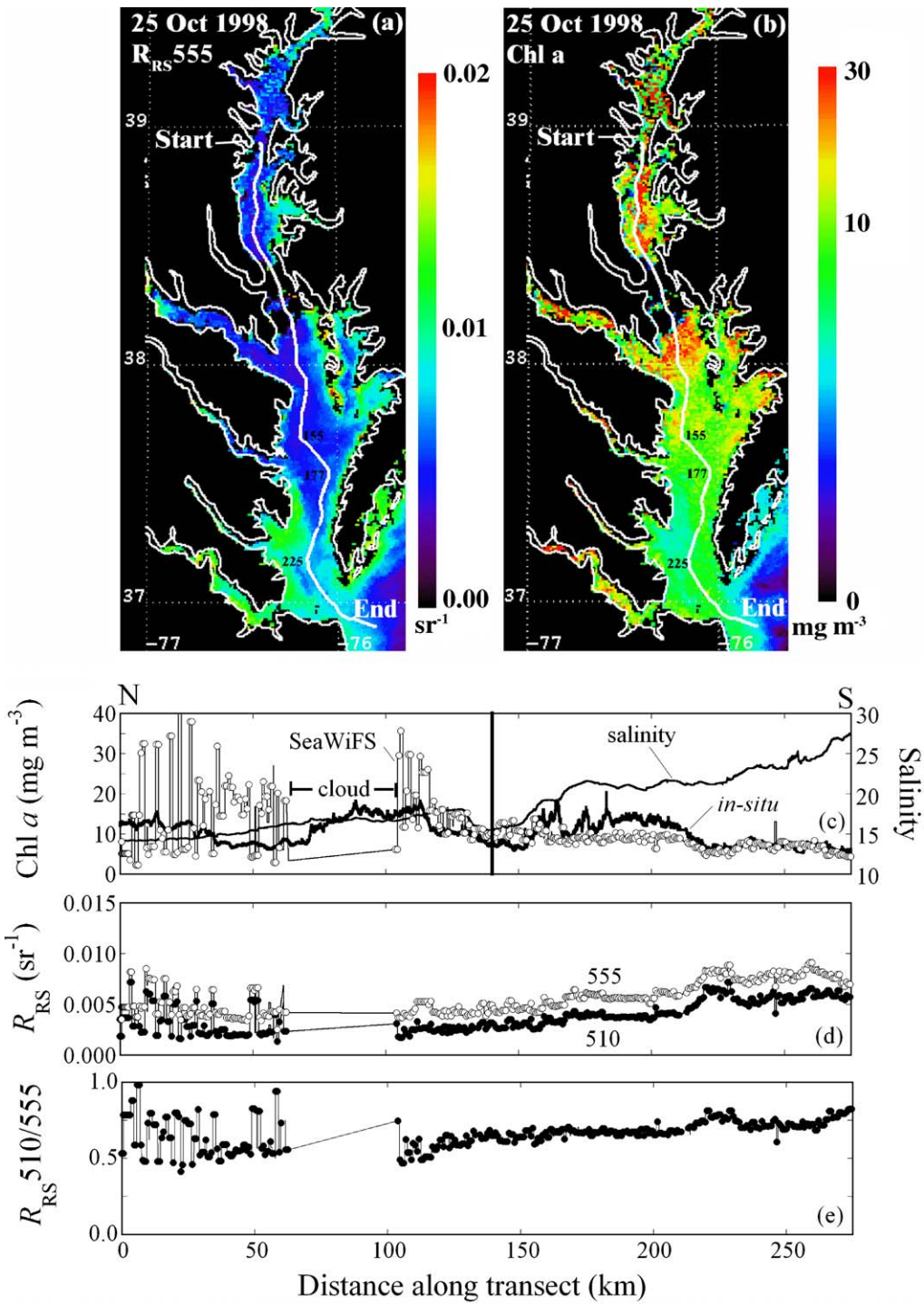

Fig. 8. (a–e) SeaWiFS images of (a) R_{RS} (555) and (b) chl *a*, 25 October 1998. Ship tracks are indicated on both images. Numbers placed along the ship track indicate distance (km) from start of transect. The solid vertical line on the chl *a* plot indicates the ship's position at time of the SeaWiFS overpass. (c–e) Comparisons of in situ salinity and chl *a* from continuous underway measurements with SeaWiFS retrievals of chl *a*: (c) salinity, in situ chl *a*, and SeaWiFS chl *a*; (d) SeaWiFS R_{RS} (510) and R_{RS} (555); (e) SeaWiFS R_{RS} 510/555 along the ship track.

4. Discussion

4.1. SeaWiFS performance in optically complex waters

This paper draws on data from satellite radiometry and in situ bio-optical measurements for Chesapeake Bay and the MAB to assess retrievals of chl *a* using the operational SeaWiFS chl *a* algorithm, OC4v.4, to support the use of SeaWiFS data for quantifying seasonal and interannual variability of phytoplankton biomass. We found that OC4v.4 applied to in situ R_{RS} overestimated in situ chl *a* in Chesapeake Bay (mean

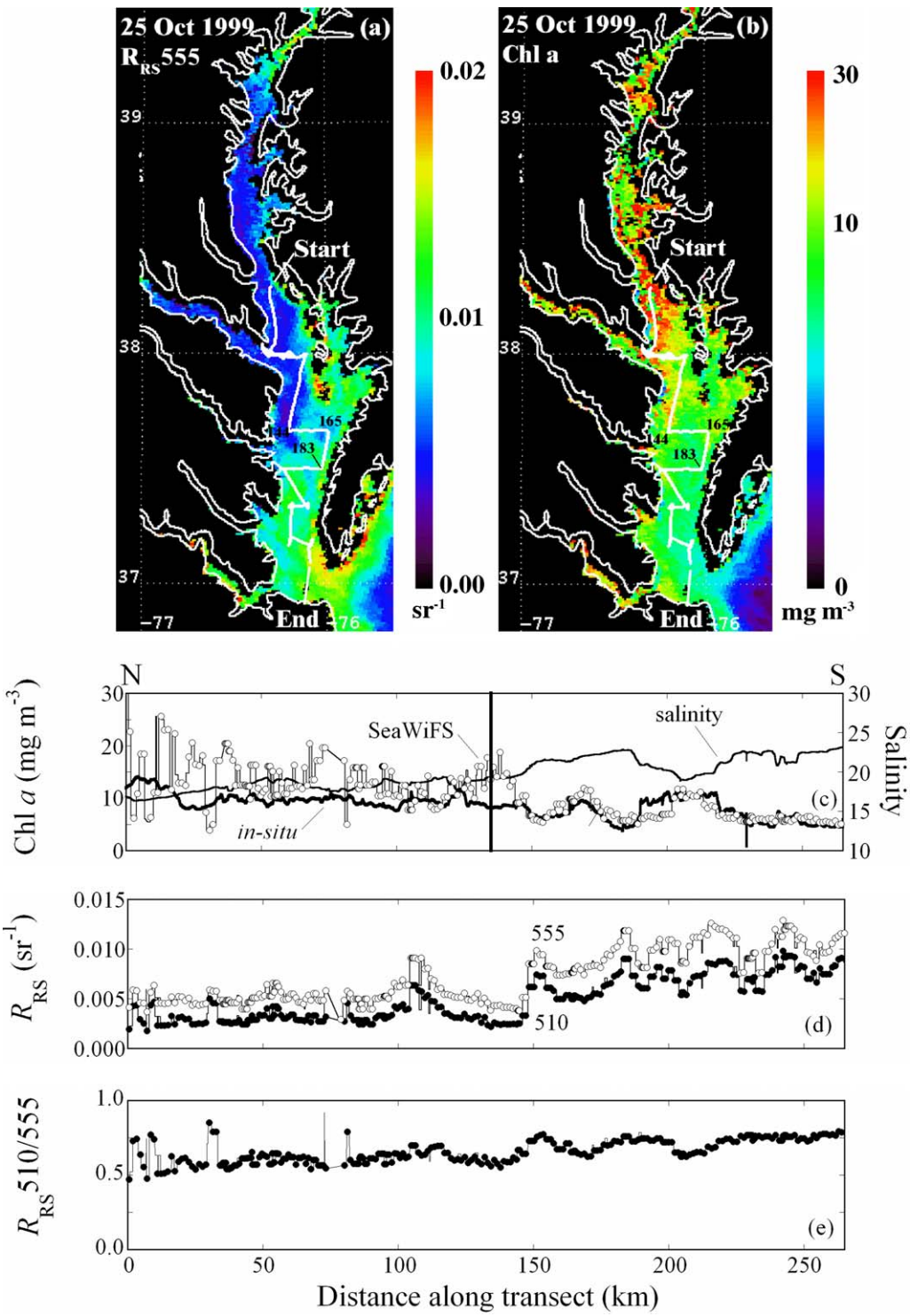

Fig. 9. (a–e) Same as Fig. 8 for 25 October 1999.

ratio 1.42 ± 1.20) (Fig. 5a). These results were not surprising as a_{cdom} and a_d were comparable in magnitude to a_{ph} (Fig. 3a,c,e). Absorption by CDOM and detritus decreases R_{RS} 510/555 such that too much absorbance is attributed to phytoplankton, and OC4v.4 thereby overestimates chl *a*. In the MAB where a_{cdom} dominated absorption at 440 nm, chl *a* retrieved from OC4v.4 applied to in situ R_{RS} showed an even larger positive bias in comparisons with in situ chl *a* (mean ratio 2.60 ± 1.36) (Fig. 5a). The high uncertainty of chl *a* obtained from OC4v.4 applied to in situ R_{RS} occurred because a_{cdom}, a_d, and a_{ph} did not co-vary in these Case 2 waters.

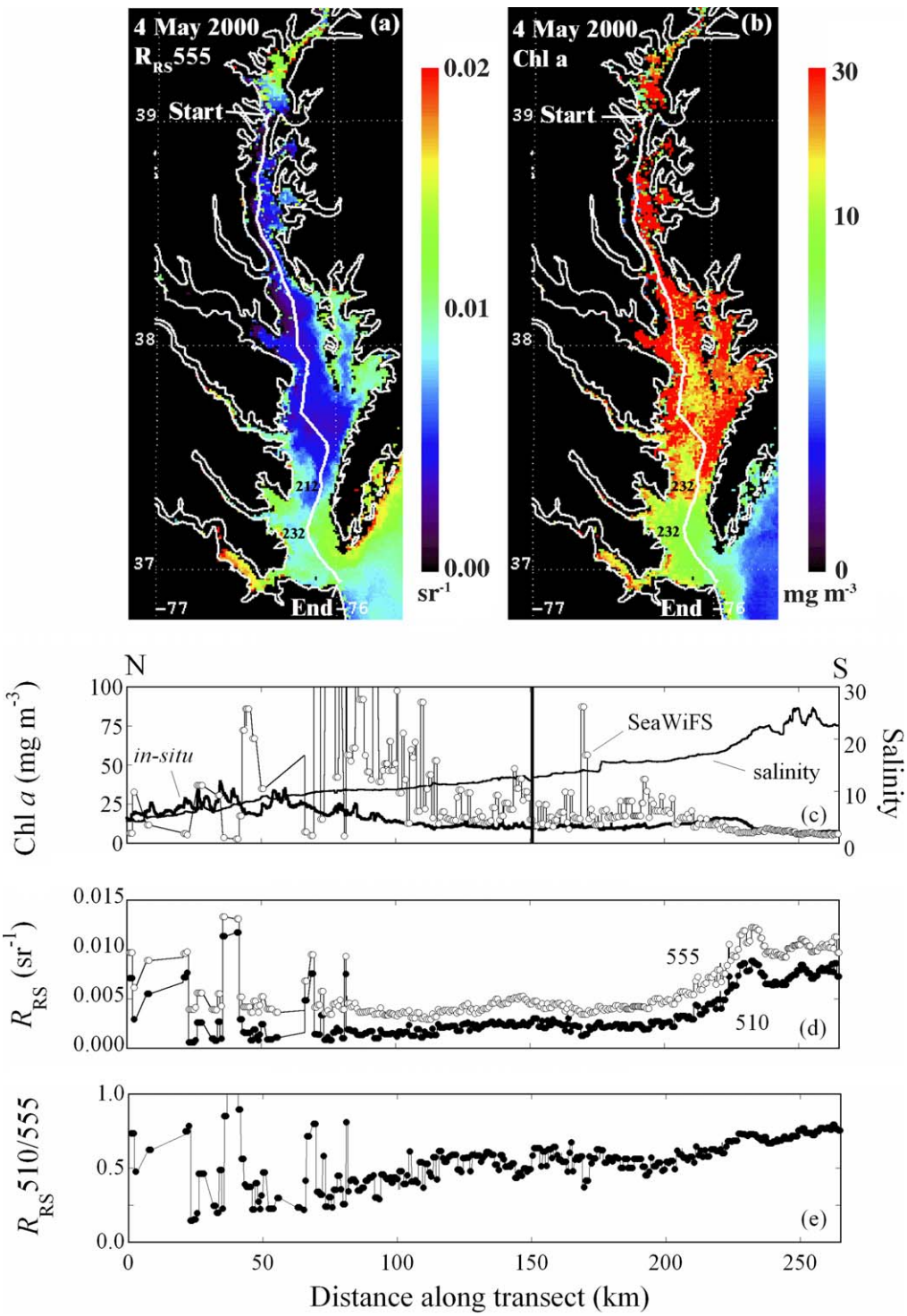

Fig. 10. (a–e) Same as Fig. 8 for 4 May 2000.

Our findings on performance of OC4v.4 in coastal waters were consistent with those reported by Ladner et al. (2002).

Both the performance of OC4v.4 and errors in satellite-derived radiances affect the accuracy of SeaWiFS retrievals of chl *a*. SeaWiFS chl *a* showed a larger, positive bias in comparisons with in situ chl *a* for the Bay (mean ratio 1.97 ± 1.85) (Fig. 5b) than we observed for chl *a* from OC4v.4 applied to in situ R_{RS} (mean ratio 1.42 ± 1.20) (Fig. 5a). We found comparable biases in the MAB for SeaWiFS retrievals of chl *a* using OC4v.4 as we did for chl *a* obtained from OC4v.4 applied to in situ R_{RS} (2.44 ± 1.16 and 2.60 ± 1.36, respectively) (Fig. 5a,b). The increased bias in the Bay can be

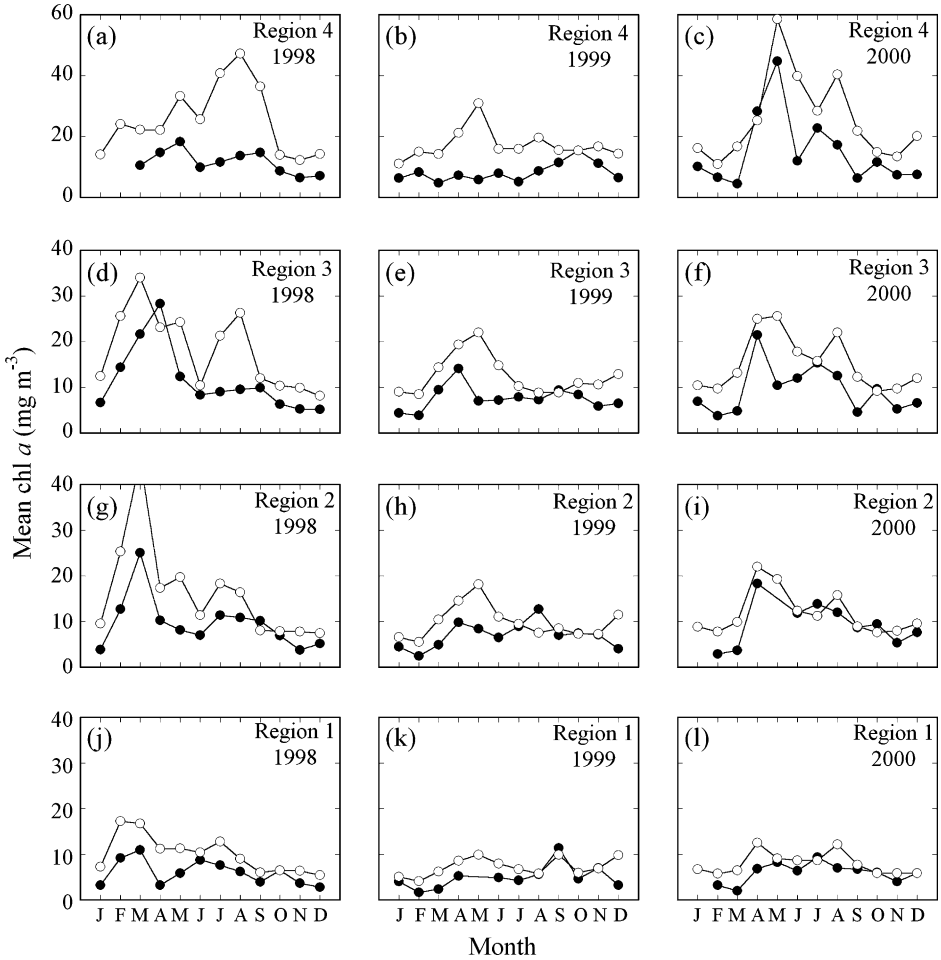

Fig. 11. (a–l) Monthly means of SeaWiFS chl *a* (open circles) and in situ chl *a* (filled circles) for regions 1–4 (Table 1). Mean values of SeaWiFS chl *a* were calculated from a mask that followed the contours of the main Bay but excluded tributaries and extended seaward of the coastline for several pixels.

explained by errors in SeaWiFS R_{RS} that would decrease the reflectance ratio, R_{RS} 510/555, used by OC4v.4 to estimate chl *a*. SeaWiFS overestimated R_{RS} (510) by ~1% and R_{RS} (555) by ~4%, based on simple, linear regressions applied to matches (Fig. 6d,e), leading to underestimates of R_{RS} 510/555 and the resulting overestimates of chl *a*. It should be noted, however, that R_{RS} matches were relatively few ($n \leq 17$), and there was significant variability about the mean ratio (ca. 15%). Whereas the average ratio of SeaWiFS R_{RS} to in situ R_{RS} at 510 nm indicated SeaWiFS overestimated R_{RS} (510), the matches showed SeaWiFS often underestimated R_{RS} (510) (Fig. 6d). Six of the 16 matches at 510 nm were above the 1:1 line, 10 of the 16 were below the 1:1 line. Approximately equal numbers of observations for R_{RS} (555) were above and below the 1:1 line, with eight above and nine below (Fig. 6e). We believe the mean ratio may be somewhat misleading as the data for matches showed SeaWiFS underestimated R_{RS} more often than it overestimated R_{RS}, and that the magnitude of underestimates increased at lower wavebands. If this small data set of matches was representative, the tendency for SeaWiFS to underestimate R_{RS} (510) to a greater extent than R_{RS} (555) would cause R_{RS} 510/555 to be lower than it should be, and chl *a* derived from OC4v.4 would be higher than it should be, thereby increasing the error (bias) between SeaWiFS chl *a* and in situ chl *a*. The lack of increased bias for comparisons of SeaWiFS chl *a* and chl *a* obtained from OC4v.4 applied to in situ R_{RS} in the MAB suggests that SeaWiFS radiances were more accurate in adjacent coastal waters than in the Bay proper, as would be expected for waters of lower turbidity typically found in the MAB. These findings suggest that differences between SeaWiFS chl *a* and in situ chl *a* in the MAB may be traced to the algorithm, rather than to errors of atmospheric correction.

4.2. Regional and seasonal variability of SeaWiFS performance

Chesapeake Bay is a highly variable environment where small-scale changes of chl *a* occur rapidly, making synoptic measurements essential to resolve phytoplankton

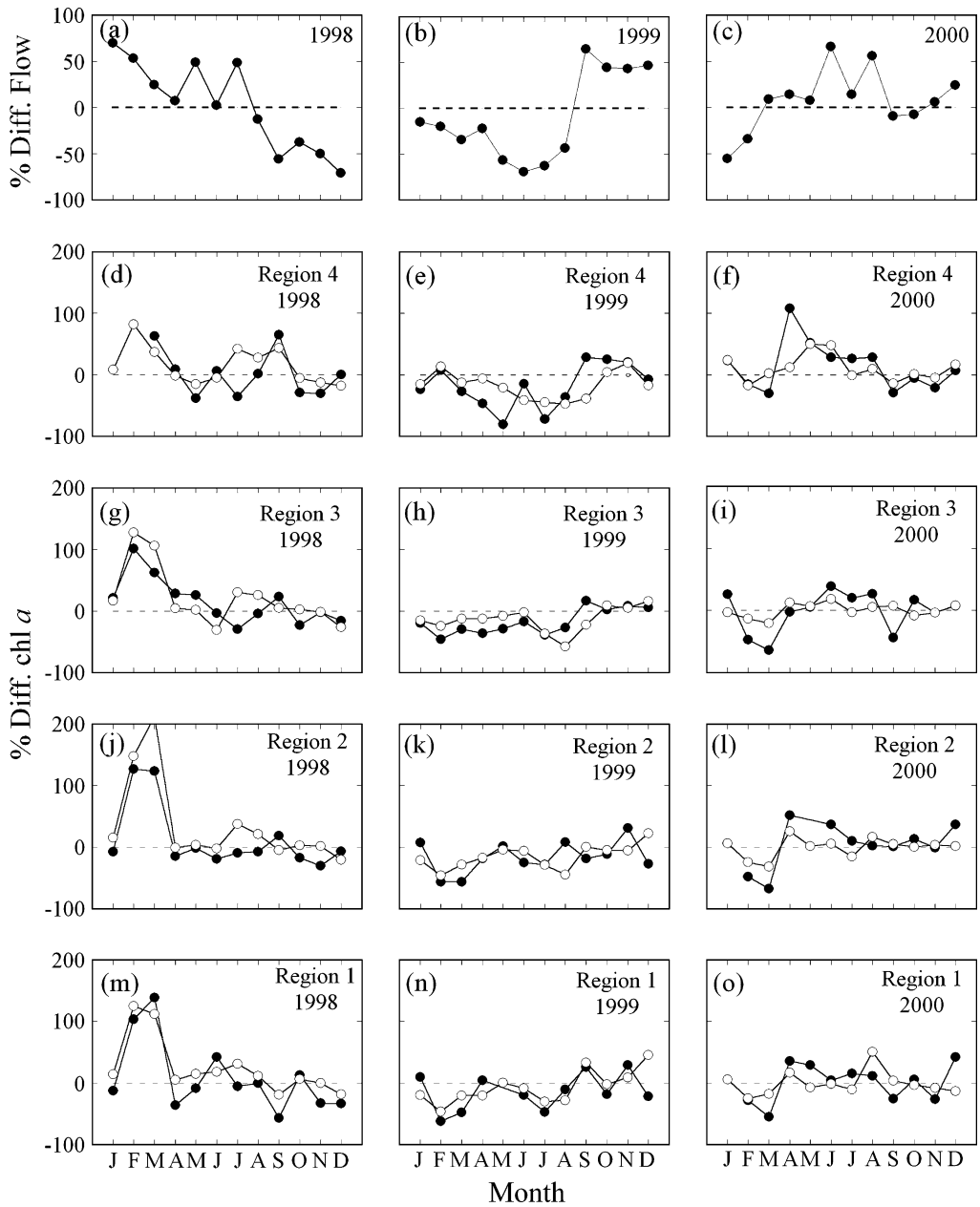

Fig. 12. (a–c) Deviations of monthly mean flow from the Susquehanna River from the 3-year (1998–2000) mean; (d–o) deviations of monthly mean SeaWiFS chl *a* (open circles) and in situ chl *a* (filled circles) from the respective 3-year (1998–2000) means. Mean values of SeaWiFS chl *a* were calculated as described in Fig. 11 legend.

dynamics. Our evaluation of SeaWiFS performance was directed at quantifying phytoplankton biomass as chl *a* at increased temporal resolution to augment extensive shipboard measurements, motivated in large part by the need to increase the frequency of sampling. Our comparisons of SeaWiFS retrievals of chl *a* using OC4v.4, chl *a* from OC4v.4 applied to in situ R_{RS}, and in situ chl *a* revealed higher uncertainty for SeaWiFS chl *a* than for estimates from in situ R_{RS} (Fig. 5a,b). The higher uncertainty for SeaWiFS chl *a* probably reflected time-space aliasing of satellite overpasses and in situ measurements, traceable to small-scale, high frequency changes of phytoplankton biomass commonly observed in the Bay. We submit that matches alone may fail to represent the performance of SeaWiFS retrievals of chl *a* in an ecosystem such as the Bay as a consequence of high spatial and temporal variability. An alternative we explored was to minimize time-space aliasing by using chl *a* data from continuous, underway transects to assess the extent to which SeaWiFS captured spatial variability. This approach allowed us to quantify the accuracies of SeaWiFS chl *a* on a regional basis.

SeaWiFS retrievals of chl *a* in the upper Bay were poor, probably due to high turbidity and low biomass,

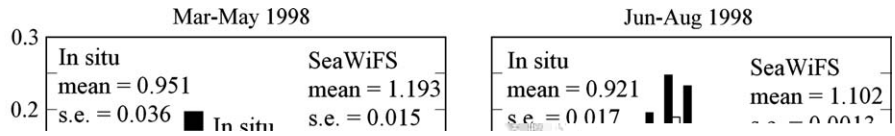

Fig. 13. (a–f) Frequency distributions of in situ and SeaWiFS chl *a* for the spring and summer seasons in Chesapeake Bay regions 1–4; (g) frequency distributions of in situ chl *a* for March, April and May of 2000, same regions.

but we found SeaWiFS R_{RS} useful to identify gradients of turbidity. R_{RS} (555) images (Figs. 8–10a) showed relatively high R_{RS} (555) in the upper Bay, low R_{RS} (555) in the mid-Bay, and high R_{RS} (555) again in the lower Bay. This axial trend of R_{RS} (555) was consistent with regional patterns of in situ R_{RS} (Magnuson et al., 2004). The upper Bay also had exceptionally high K_d (490) and a_d, indicating high turbidity and the potential for increased scattering (Fig. 3c,g). The transition from high R_{RS} (555) in the upper Bay to relatively low R_{RS} (555) in the mid-Bay occurred from $\sim$39.4° to 39.0°N where the estuarine turbidity maximum (ETM) is typically found (Roman et al., 2001). The ETM is a region of elevated suspended sediment and reduced light availability associated with the landward limit of salt intrusion (Schubel, 1968). Such gradients of turbidity and light attenuation have been found to delineate the northern boundary of the spring bloom, and are known to migrate in response to freshwater flow (Harding, 1994). Figs. 8–10a indicated some north-south variability of the gradient of R_{RS} (555). The gradient was farthest north in the 25 October 1998 image (Fig. 8a), a time of very low freshwater flow into the Bay, and was farthest south in the 4 May 2000 image (Fig. 10a), during a time of high spring flow. These images suggest that SeaWiFS R_{RS} may be useful to track the axial migration of the ETM, and therefore the landward boundary of the spring bloom.